

Gas-Phase Separations of Protein and Peptide Ion Fragments Generated by Collision-Induced Dissociation in an Ion Trap

Ethan R. Badman,[†] S. Myung, and David E. Clemmer*

Department of Chemistry, Indiana University, Bloomington, Indiana 47405

Ion mobility/time-of-flight mass spectrometry techniques have been used to examine distributions of fragment ions generated by collision-induced dissociation (CID) in a quadrupole ion trap. The mobility-based separation step prior to mass-to-charge (m/z) analysis reduces spectral congestion and provides information that complements m/z -based assignments of peaks. The approach is demonstrated by examining fragmentation patterns of insulin chain B (a 30-residue peptide), and ubiquitin (a protein containing 76 amino acids). Some fragments of ubiquitin show evidence for multiple stable conformations.

Mass spectrometry (MS) techniques and tandem (MS/MS or MSⁿ)^{1,2} strategies can provide detailed structural information about many different types of ions, including those generated from peptides,^{3–5} proteins,^{6–11} and carbohydrates.^{12–14} Recently, a number of groups have investigated the ability to determine information about sequences from dissociating whole proteins, an approach that is referred to as *top-down sequencing*.⁹ The ability to generate and assign fragments directly from protein parent ions offers several potential advantages, as compared with proteolytic approaches. For example, none of the solution chemistry associated with digestion and cleanup is required. Moreover, the entire protein sequence is potentially available from MS/MS analysis of

the intact protein, whereas regions of sequence are often lost upon digestion and sample clean up.

With this in mind, a variety of activation methods and instrumental configurations^{6–11,15–20} have been used to produce and analyze fragment ions from whole proteins. After activation and dissociation are achieved, a significant issue in these systems is the complex pattern of peaks that arises from dissociation of multiply charged ions. Fragment ions may exist over a range of charge states and sizes, and peak assignments are often complicated by the inability to resolve isotopic structure in high-charge state fragments, as well as overlapping peaks associated with different fragments.

Two strategies appear particularly well-suited for reducing spectral congestion in these systems. High-resolution techniques, such as Fourier transform (FT) MS often allow isotopic peaks (as well as overlapping isotope distributions from multiple ions) to be resolved, even for high-charge state fragments.^{9,10} Additionally the high-mass accuracy associated with FTMS measurements is valuable for assigning peaks. Another approach that has emerged as a means of reducing spectral congestion involves exposing highly charged fragments to oppositely charged ions (ion/ion reactions).²⁰ As protons are removed from high-charge state fragment ions, peaks are shifted to higher m/z values, reducing spectral congestion and removing ambiguities associated with assigning charge states.^{8,11,20} The kinetics of charge reduction is such that high-charge-state ions react faster than low-charge-state ions; it is possible to rapidly reduce a distribution of charge states and fragments to primarily singly and doubly charged ions.

In this paper, we present an alternative strategy for reducing spectral congestion upon dissociation of multiply charged proteins, a combined ion mobility/time-of-flight (TOF) mass spectrometry approach to analysis of fragments that are produced from collision-induced dissociation in an ion trap. The mobility-based separation of fragment ions that can be carried out prior to MS analysis appears to be an advantage that is unique to the injected-ion drift tube configuration. The separation reduces spectral congestion

[†] Current address: Department of Chemistry, Purdue University, West Lafayette, IN 47907-1393.

- (1) McLuckey, S. A. *J. Am. Soc. Mass Spectrom.* **1992**, *3*, 599–614.
- (2) Shukla, A. K.; Futrell, J. H. *J. Mass Spectrom.* **2000**, *35*, 1069–1090.
- (3) Papayannopoulos, I. A. *Mass Spectrom. Rev.* **1995**, *14*, 49–73.
- (4) Martin, S. E.; Shabanowitz, J.; Hunt, D. F.; Marto, J. A. *Anal. Chem.* **2000**, *72*, 4266–4274.
- (5) Masselon, C.; Anderson, G. A.; Harkewicz, R.; Bruce, J. E.; Pasa-Tolic, L.; Smith, R. D. *Anal. Chem.* **2000**, *72*, 1918–1924.
- (6) Loo, J. A.; Edmonds, C. G.; Smith, R. D. *Science* **1990**, *248*, 201–204.
- (7) Wu, Q. Y.; Vanorden, S.; Cheng, X. H.; Bakhtiar, R.; Smith, R. D. *Anal. Chem.* **1995**, *67*, 2498–2509.
- (8) Stephenson, J. L.; Cargile, B. J.; McLuckey, S. A. *Rapid Commun. Mass Spectrom.* **1999**, *13*, 2040–2048.
- (9) Kelleher, N. L.; Lin, H. Y.; Valaskovic, G. A.; Aaserud, D. J.; Fridriksson, E. K.; McLafferty, F. W. *J. Am. Chem. Soc.* **1999**, *121*, 806–812.
- (10) Zubarev, R. A.; Horn, D. M.; Fridriksson, E. K.; Kelleher, N. L.; Kruger, N. A.; Lewis, M. A.; Carpenter, B. K.; McLafferty, F. W. *Anal. Chem.* **2000**, *72*, 563–573.
- (11) Reid, G. E.; Wu, J.; Chrisman, P. A.; Wells, J. M.; McLuckey, S. A. *Anal. Chem.* **2001**, *73*, 3274–3281.
- (12) Reinhold, V. N.; Reinhold, B. B.; Costello, C. E. *Anal. Chem.* **1995**, *67*, 1772–1784.
- (13) Solouki, T.; Reinhold, B. B.; Costello, C. E.; O'Malley, M.; Guan, S. H.; Marshall, A. G. *Anal. Chem.* **1998**, *70*, 857–864.
- (14) Harvey, D. J. *J. Mass Spectrom.* **2000**, *35*, 1178–1190.

- (15) Little, D. P.; Speir, J. P.; Senko, M. W.; O'Connor, P. B.; McLafferty, F. W. *Anal. Chem.* **1994**, *66*, 2809–2815.
- (16) Senko, M. W.; Speir, J. P.; McLafferty, F. W. *Anal. Chem.* **1994**, *66*, 2801–2808.
- (17) Chorush, R. A.; Little, D. P.; Beu, S. C.; Wood, T. D.; McLafferty, F. W. *Anal. Chem.* **1995**, *67*, 1042–1046.
- (18) Price, W. D.; Schnier, P. D.; Williams, E. R. *Anal. Chem.* **1996**, *68*, 859–866.
- (19) Jockusch, R. A.; Schnier, P. D.; Price, W. D.; Strittmatter, E. F.; Demirev, P. A.; Williams, E. R. *Anal. Chem.* **1997**, *69*, 1119–1126.
- (20) Stephenson, J. L.; McLuckey, S. A. *Anal. Chem.* **1998**, *70*, 3533–3544.

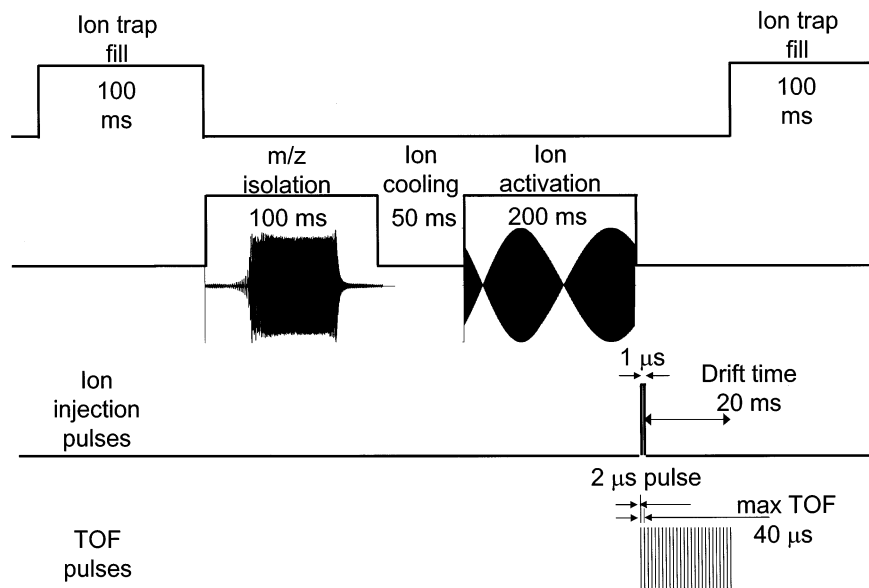


Figure 1. Experimental timing diagram for the ion trap MS/MS/ion mobility/TOF experiment. Ions are injected into the ion trap from the ion source for 100 ms. MS/MS in the ion trap is achieved using a 100-ms ion isolation period, followed by a 50-ms ion cooling time and a 200-ms activation period. Example isolation and activation waveforms are shown for the MS/MS step (only one waveform is shown for each step, although multiple pulses are used). After the 200-ms activation period, the 1- μ s injection pulse of ions into the drift tube is initiated by pulsing the ion trap end cap closest to the drift tube. Time-of-flight pulses are synchronized with the drift pulse and occur at 40- μ s intervals during the entire 20-ms drift time measurement window.

and in favorable cases provides information about the fragment ion charge state. Additionally, we find that some large fragment ions appear to exist as multiple conformations. Here, we discuss the initial development of the approach and early findings by examining fragment ions generated from dissociation of insulin chain B and ubiquitin.

The present work is closely related to a number of other types of studies, including a flurry of activity associated with the analysis of complex biomolecular systems with mobility-based techniques.^{21–30} Particularly relevant to the present study is an ion trap/ion mobility geometry instrument described by Creaser et al.³¹ This configuration has MS/MS capabilities prior to the drift tube and has been used to examine the structures of some small organic ions. The generation of peptide ion fragments in a trap of a tandem quadrupole ion trap/time-of-flight instrument has also been described by Lubman and co-workers.^{32,33} A number of other

studies have described advantages associated with collision induced dissociation upon injection into the drift tube or upon exiting the drift tube.^{34–39}

EXPERIMENTAL SECTION

General. Ion mobility separations and combinations of ion mobility with MS techniques have been reviewed previously.^{40–42} Only a brief overview of these experimental methods is presented here. Experiments were performed using a home-built electrospray ionization (ESI) quadrupole ion trap/injected-ion mobility/TOF mass spectrometer, described previously.³⁶ Positive (protonated) ions formed by ESI are focused and accumulated into an ion trap for 100 ms. A specific m/z ion is then selected and energized as described below, and the subsequent fragments that are produced are ejected into the drift tube. The sequence of applied waveforms and pulses used in this experiment are shown in Figure 1 (and discussed in more detail below). Here, we utilize an injected ion drift tube geometry that is similar to a design

(21) Wyttenbach, T.; von Helden, G.; Bowers, M. T. *J. Am. Chem. Soc.* **1996**, *118*, 8355–8364.

(22) Shelimov, K. B.; Jarrold, M. F. *J. Am. Chem. Soc.* **1997**, *119*, 2987–2994.

(23) Woenckhaus, J.; Mao, Y.; Jarrold, M. F. *J. Phys. Chem. B* **1997**, *101*, 847–851.

(24) Srebalus, C. A.; Li, J. W.; Marshall, W. S.; Clemmer, D. E. *Anal. Chem.* **1999**, *71*, 3918–3927.

(25) Wu, C.; Klasmeier, J.; Hill, H. H. *Rapid Commun. Mass Spectrom.* **1999**, *13*, 1138–1142.

(26) Wu, C.; Siems, W. F.; Klasmeier, J.; Hill, H. H. *Anal. Chem.* **2000**, *72*, 391–395.

(27) Purves, R. W.; Barnett, D. A.; Guevremont, R. *Int. J. Mass Spectrom.* **2000**, *197*, 163–177.

(28) Counterman, A. E.; Hilderbrand, A. E.; Barnes, C. A. S.; Clemmer, D. E. *J. Am. Soc. Mass Spectrom.* **2001**, *12*, 1020–1035.

(29) Wyttenbach, T.; Kemper, P. R.; Bowers, M. T. *Int. J. Mass Spectrom.* **2001**, *212*, 13–23.

(30) Purves, R. W.; Barnett, D. A.; Ells, B.; Guevremont, R. *J. Am. Soc. Mass Spectrom.* **2001**, *12*, 894–901.

(31) Creaser, C. S.; Benyazzar, M.; Griffiths, J. R.; Stygall, J. W. *Anal. Chem.* **2000**, *72*, 2724–2729.

(32) Qian, M. G.; Lubman, D. M. *Rapid Commun. Mass Spectrom.* **1996**, *10*, 1911–1920.

(33) Jin, X. Y.; Kim, J.; Parus, S.; Lubman, D. M.; Zand, R. *Anal. Chem.* **1999**, *71*, 3591–3597.

(34) Liu, Y. S.; Clemmer, D. E. *Anal. Chem.* **1997**, *69*, 2504–2509.

(35) Hoaglund-Hyzer, C. S.; Li, J. W.; Clemmer, D. E. *Anal. Chem.* **2000**, *72*, 2737–2740.

(36) Hoaglund-Hyzer, C. S.; Clemmer, D. E. *Anal. Chem.* **2001**, *73*, 177–184.

(37) Hoaglund-Hyzer, C. S.; Lee, Y. J.; Counterman, A. E.; Clemmer, D. E. *Anal. Chem.* **2001**, *74*, 992–1006.

(38) Stone, E.; Gillig, K. J.; Ruotolo, B.; Fuhrer, K.; Gonin, M.; Schultz, A.; Russell, D. H. *Anal. Chem.* **2001**, *73*, 2233–2238.

(39) Stone, E. G.; Gillig, K. J.; Ruotolo, B. T.; Russell, D. H. *Int. J. Mass Spectrom.* **2001**, *212*, 519–533.

(40) St Louis, R. H.; Hill, H. H. *Crit. Rev. Anal. Chem.* **1990**, *21*, 321–355.

(41) Hoaglund-Hyzer, C. S.; Counterman, A. E.; Clemmer, D. E. *Chem. Rev.* **1999**, *99*, 3037–3079.

(42) Jarrold, M. F. *Annu. Rev. Phys. Chem.* **2000**, *51*, 179–207.

described previously. A 100 V potential drop was used to inject ions into the drift tube. The drift region is 50.6 cm long and is operated with ~ 2.0 Torr of 300 K He buffer gas. The applied field in the drift region is 12.85 V cm^{-1} . As parent and fragment ions drift through the drift tube, they are separated on the basis of differences in their mobilities, which depend on the overall collision cross-section and charge state.

Ions that exit the drift tube are focused into the source region of an orthogonal reflectron geometry TOF mass spectrometer. High-voltage pulses synchronous with the drift pulse are used to initiate flight time measurements in the TOF instrument. As described previously, because drift times (0–10 ms) are much longer than flight times ($< 40 \mu\text{s}$ in the present study), it is possible to record information about mobilities and flight time distributions for the mixture of ions in a single experimental sequence. We refer to this as a nested drift (flight) time measurement.⁴³ Flight times are converted to m/z values by using a standard multipoint calibration. Unless otherwise noted, we delineate peaks in two dimensions by giving $t_d(m/z)$ values, similar to the nomenclature we have proposed previously for nested data.

Ion Storage, m/z Selection, and Collisional Activation in the Ion Trap. Quadrupole ion traps have been used extensively for MS/MS and MS^n experiments.⁴⁴ Numerous approaches for isolation and activation of parent ions have been described, including stored-waveform inverse Fourier transform (SWIFT),^{45–47} filtered noise fields,⁴⁸ and dc or random noise pulses (for activation only).^{49,50} Trapped ions oscillate at secular frequencies characteristic of their mass-to-charge ratios (under fixed operating conditions),⁵¹ and in all of these approaches, application of a waveform resonantly excites the ions at their frequencies of oscillation and causes them to be activated or ejected, depending on the amplitude of the waveform. Secular frequencies can be calculated using measurable experimental parameters and the Mathieu equation⁵¹ for ion stability in the trap. By constructing waveforms that include the sum of all of the frequencies of motion of the ions to be ejected, mass isolation of a desired (nonresonant) ion can be achieved. For collisional activation of a specific ion (or mixtures of ions), low-amplitude resonance frequency waveforms are used to excite (but not eject) ions. In this way, ions are slowly heated as they undergo multiple energizing collisions with the buffer gas. As ions dissociate, the fragments that are formed are no longer resonant with the excitation pulse; thus, they should thermalize and accumulate in the center of the trap.

The present studies utilize a quadrupole ion trap (model C-125, R. M. Jordan, Grass Valley, CA) at the front of an injected ion drift tube, as described previously for use as an ion storage

device.⁵² The trap is operated with ~ 1.0 mTorr of room-temperature helium buffer gas and an applied rf trapping voltage of 1300–1500 V_{0-p} , corresponding to a low mass trapping limit of $m/z \sim 150$. Ions are selected and subsequently energized by applying constructed waveforms to one of the ion trap endcap electrodes. The other endcap electrode is pulsed to eject ions from the trap and into the drift tube. The resonance frequencies used for parent ion isolation and collision-induced dissociation are calculated using the Mathieu equation. After determination of the frequencies for isolation and excitation, SWIFT⁵³ waveforms are generated using ICR-2LS software (version 2.18).⁵⁴ Waveforms were 8192 points long and generated at a sampling rate of 1.25 MHz, resulting in frequency spacing of 152.6 Hz. Waveforms are downloaded from the PC to an arbitrary waveform generator (model 195, 4 channel output, Wavetek-Datron, San Diego, CA), and the output of the waveform generator then passes first through a TTL-switching box then a float box before being applied to the ion trap endcap electrode. The switching box uses a TTL pulse to control which of two outputs from the waveform generator is applied to the endcap electrode. The float box allows the dc bias on the ion trap to be added to the waveform; the sum is applied to the endcap electrode.

Figure 1 shows a schematic representation of the timing diagram for the ion trap/drift tube/TOF experiment. The SWIFT pulses for ion isolation are applied after the 100-ms ion injection period using multiple pulses (typically 14, for a total time of ~ 100 ms) at ~ 6.0 – $8.0 V_{0-p}$ to minimize parent ion ejection. Typical isolation waveform notch bandwidths are centered on the most abundant isotope of the parent ion of interest over a range of $\pm 4 m/z$. A 50-ms cooling time follows the ion isolation step. We have used long times and low amplitude activation for CID, which has been determined to be the most effective method for obtaining MS/MS spectra with minimal ion ejection.²⁰ The activation waveform for these experiments is applied for 200 ms at amplitudes of ~ 0.8 – $1.5 V_{0-p}$. Activation waveforms are constructed to resonantly excite a ~ 300 Hz frequency band centered on the secular frequency of the parent ion.

Ion Production. Ions are produced at atmospheric pressure by electrospraying ~ 30 to $60 \mu\text{M}$ solutions (49:49:2 or 69:29:2 water/methanol/acetic acid of insulin chain B or ubiquitin, respectively). The charged species enter a variable-temperature differentially pumped desolvation region through a 5-cm-long 0.32-cm diameter tube; ions exit the desolvation region directly into the main vacuum chamber. Insulin chain B (oxidized, 80% purity, Sigma) and bovine ubiquitin (90% purity, Sigma) were used without further purification.

RESULTS AND DISCUSSION

Isolation and Activation of Oxidized Insulin Chain B Ions.

Figure 2 shows example mass spectra associated with typical MS and MS/MS analyses for oxidized insulin chain B, a 30-amino acid peptide (with a sequence of FVNQHLGSH LVEALYLVCGERGFFYTPKA and having an average isotopic mass of 3495.7 Da). Under the ESI conditions that are employed, the mass spectrum

(43) Hoaglund, C. S.; Valentine, S. J.; Sporleder, C. R.; Reilly, J. P.; Clemmer, D. E. *Anal. Chem.* **1998**, *70*, 2236–2242.

(44) McLuckey, S. A.; Glish, G. L.; Vanberkel, G. J. *Int. J. Mass Spectrom. Ion Process.* **1991**, *106*, 213–235.

(45) Julian, R. K.; Cooks, R. G. *Anal. Chem.* **1993**, *65*, 1827–1833.

(46) Guan, S. H.; Marshall, A. G. *Anal. Chem.* **1993**, *65*, 1288–1294.

(47) Doroshenko, V. M.; Cotter, R. J. *Rapid Commun. Mass Spectrom.* **1996**, *10*, 65–73.

(48) Goeringer, D. E.; Asano, K. G.; McLuckey, S. A.; Hoekman, D.; Stiller, S. W. *Anal. Chem.* **1994**, *66*, 313–318.

(49) Lammert, S. A.; Cooks, R. G. *Rapid Commun. Mass Spectrom.* **1992**, *6*, 528–530.

(50) McLuckey, S. A.; Goeringer, D. E.; Glish, G. L. *Anal. Chem.* **1992**, *64*, 1455–1460.

(51) March, R. E. *J. Mass Spectrom.* **1997**, *32*, 351–369.

(52) Hoaglund, C. S.; Valentine, S. J.; Clemmer, D. E. *Anal. Chem.* **1997**, *69*, 4156–4161.

(53) Marshall, A. G.; Wang, T.-C. L.; Ricca, T. L. *J. Am. Chem. Soc.* **1985**, *107*, 7893–7897.

(54) Anderson, G. A.; Bruce, J. E.; Smith, R. D., 1996.

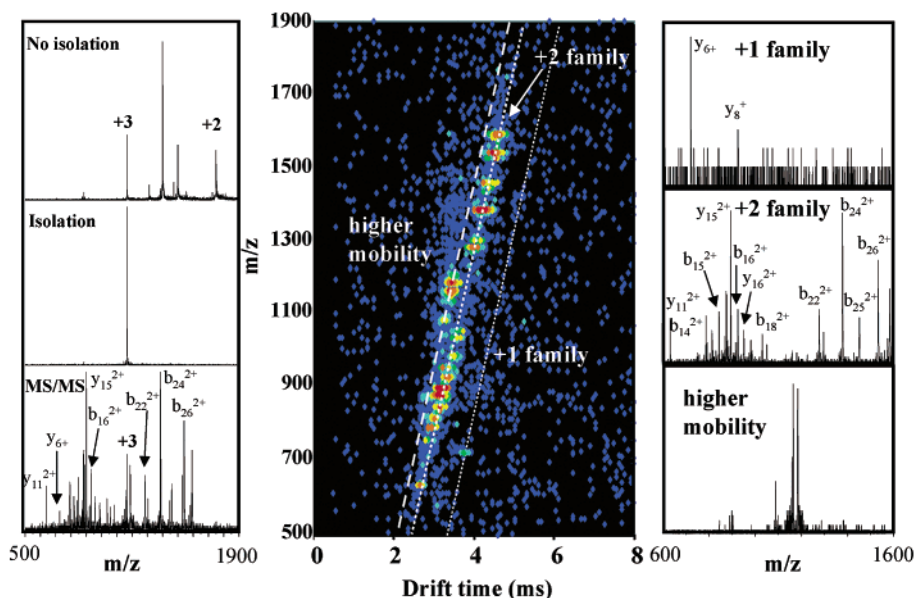


Figure 2. (left) Spectra for insulin chain B showing the initial mass spectrum (top), isolation of the 3+ charge state (middle), and fragment ion spectrum of the isolated 3+ charge state (bottom). The mass spectra were obtained by integrating the two-dimensional data over all drift times. (middle) Nested drift(flight) time for the dissociation of insulin chain B 3+. The charge state families for the higher mobility 2+ and 1+ ions are shown with the dashed lines (from left to right, respectively) used here as visual guides. (right) The 1+, 2+, and higher mobility fragment ion families from the dissociation of the 3+ ion of insulin chain B obtained by taking diagonal slices through the nested drift(flight) time distribution.

is dominated by four peaks; the $[M + 3H]^{3+}$ and $[M + 2H]^{2+}$ parent ions are observed at m/z values of 1166.2 and 1748.8, respectively. Application of the isolation waveform makes it possible to select specific ions, as shown in Figure 2, for the example selection of the $[M + 3H]^{3+}$ peak. Subsequent activation of these ions leads to the MS/MS fragmentation spectrum (also shown in Figure 2). Under the conditions that are employed, more than 80% of the parent ions typically dissociate to fragments. Because the sequence of this peptide is known, it is straightforward to identify many anticipated fragment ions.

Nested Drift(Flight) Time Distributions for the CID Fragments of Oxidized Insulin Chain B. Figure 2 also shows nested $t_d(m/z)$ data for the distribution of fragment ions that is obtained upon isolation and collisional activation of the $[M + 3H]^{3+}$ parent. In these data, m/z values for most of the peaks that fall along the central family of ions show that this family corresponds to doubly charged fragments. Several peaks, including the $[M + 3H]^{3+}$ precursor [at $t_d(m/z) = 3.45(1166.3)$], and several other peaks at 3.09(884.7), 3.23(880.8), 3.23(1084.7), and 3.45(1161.3) have mobilities that are higher than those for the 2+ family. A single small peak [at $t_d(m/z) = 3.73(726.4)$] corresponds to the singly charged y_6 fragment. Overall, these data show that the fragment ions are separable into charge state families, as observed previously for distributions of peptide parent ions.^{55,56}

It is possible to integrate the ion intensities in the two-dimensional dataset over narrow regions to obtain distributions for specific ions. We noted previously that this type of analysis can substantially reduce chemical noise and allow small peaks to be observed, even when substantially more intense ions are

present at the same m/z ratios.^{28,57} In the case of the fragment ions that are generated in the trap, it is useful to integrate over regions of the data (centered around the dashed lines in Figure 2) associated with the single-, double-, and higher-mobility ions. Each of the mass spectra obtained in this way can be compared to the fragmentation mass spectrum obtained without mobility separation. In the case of the 1+ ions, the selective integration provides evidence for a small feature associated with the y_8 fragment that is not observed without separation. Additionally, as we have noted before, the isolation into charge state families can be useful for assigning peaks when isotope distributions are not resolved.

Nested Drift(Flight) Time Distributions for Fragments of the $[M + 6H]^{6+}$ and $[M + 7H]^{7+}$ Charge States of Ubiquitin.

ESI of solutions containing ubiquitin (with a sequence of MQIFVK-TLTG KTITLVEVPS DTIENVKAKI QDKEGIPPDQ QRLIF-AGKQL EDGRTLSDYN IQKESTLHLV LRLRGG) typically produces the 5+ to 13+ charge states. Figure 3 shows the drift(flight) time distribution that is obtained upon mass selection and activation of the $[M + 6H]^{6+}$ ions. Under the conditions that are employed, the fragmentation pattern is dominated by peaks at $t_d(m/z) = 4.41(1617.8)$ and $4.38(1634.0)$ that can be assigned to the b_{58}^{4+} and y_{58}^{4+} ions, respectively. Additionally, a number of smaller fragments are observed and can be assigned, as shown in Figures 3 and 4. As discussed above, the mobility separation allows some peaks to be clearly resolved, even though the separation of the charge state families decreases with increasing charge state. For example, in Figure 3, two of the m/z peaks have been labeled with two fragment ion assignments, y_{59}^{4+}/b_{30}^{2+} and y_{61}^{4+}/b_{46}^{3+} , because there are two possible assignments for each peak that are within $m/z \sim 0.1$ and 0.04 , respectively, of each other

(55) Valentine, S. J.; Counterman, A. E.; Hoaglund, C. S.; Reilly, J. P.; Clemmer, D. E. *J. Am. Soc. Mass Spectrom.* **1998**, *9*, 1213–1216.

(56) Henderson, S. C.; Valentine, S. J.; Counterman, A. E.; Clemmer, D. E. *Anal. Chem.* **1999**, *71*, 291–301.

(57) Taraszka, J. A.; Counterman, A. E.; Clemmer, D. E. *Fresenius' J. Anal. Chem.* **2001**, *369*, 234–245.

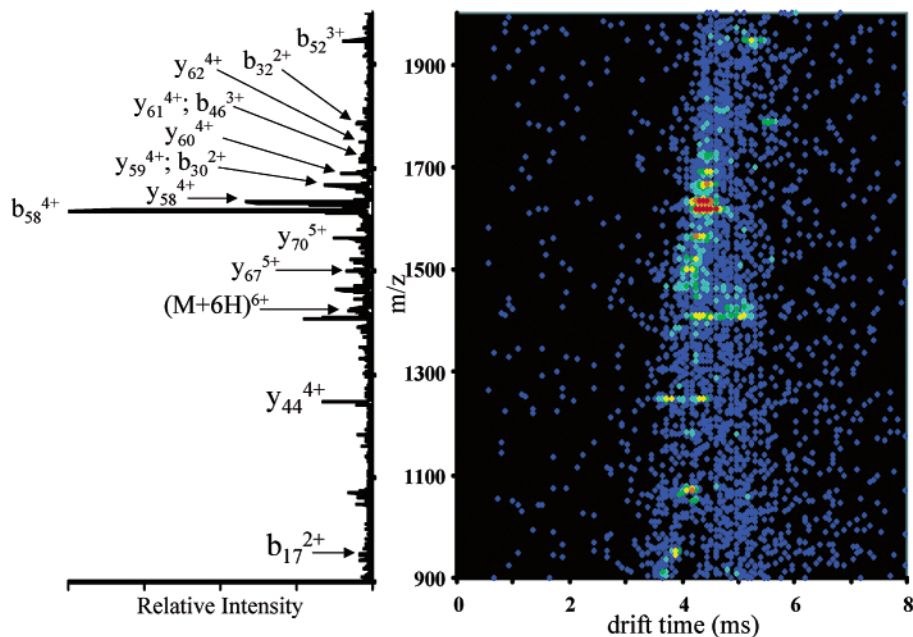


Figure 3. Nested drift(flight) time spectra for MS/MS of the $[M + 6H]^{6+}$ ion of ubiquitin. Left: summed mass spectrum over all drift times.

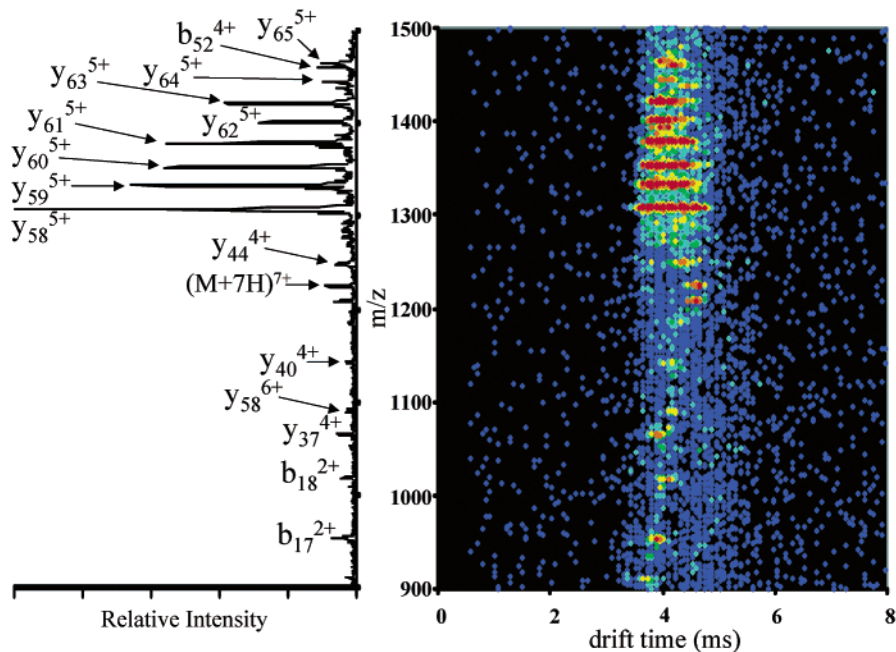


Figure 4. Nested drift(flight) time spectra for MS/MS of the $[M + 7H]^{7+}$ ion of ubiquitin. Left: summed mass spectrum over all drift times.

that cannot be resolved. These peaks can be assigned as the y_{59}^{4+} and y_{61}^{4+} , because they fall within the same mobility family as the other 4+ fragment ions observed and not within the families for the 2+ or 3+ ions (note the drift times of the b_{17}^{2+}/b_{32}^{2+} pair and the b_{52}^{3+} ions).

More insight into the fragmentation of ubiquitin comes from examining the two-dimensional dataset shown in Figure 4 that was recorded for fragments generated from the $[M + 7H]^{7+}$ precursor. The six largest peaks in this distribution correspond to a series of related fragments y_{58}^{5+} – y_{63}^{5+} . These fragments arrive over a wide range of drift times, and it is instructive to consider the ion mobility distributions for these features in more detail. Figure 5 shows the intensities of the individual y-series fragments as a function of the measured drift times. The distribution for the

y_{58}^{5+} ion shows evidence for three peaks (in roughly equal abundance). This indicates that at least three types of conformations are stable over the millisecond drift times of these experiments for this fragment. These conformers appear to exist as a family of related structural types, and the relative abundances of different conformers vary with fragment length. For example, the y_{59}^{5+} ion appears to favor less of the largest cross section conformer. For longer fragments, the distribution shifts such that the most compact form is favored.

Finally, we note that the distribution of some fragment ion conformations appears to be influenced by precursor ion charge state. Figure 6 shows drift time distributions recorded for the y_{44}^{4+} fragment upon activating either the $[M + 6H]^{6+}$ or $[M + 7H]^{7+}$ precursors. When the y_{44}^{4+} fragment is produced from the $[M +$

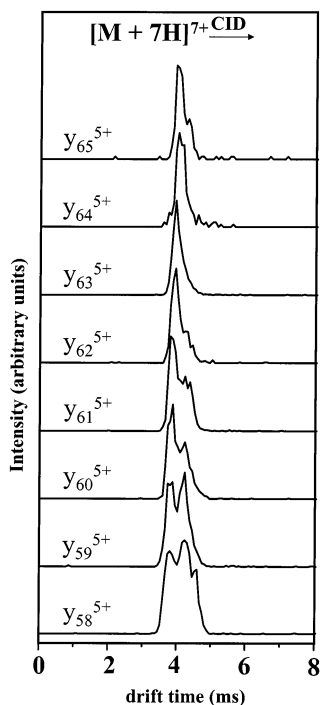


Figure 5. Drift time distributions for the y_{58}/y_{65}^{5+} fragment ions from dissociation of the $[M + 7H]^{7+}$ parent ion of ubiquitin showing evidence for multiple conformers of fragment ions.

$6H]^{6+}$ parent, the abundances of the relatively compact and open forms of this ion are 44 and 56%; however, dissociation of the $[M + 7H]^{7+}$ conformer clearly favors the more open conformer. As shown in Figures 3 and 4, and seen in previous work,¹¹ there are some significant differences in the identities and relative abundances of the fragment ions observed from the 7+ to 6+ parent ions. This effect might be explained by considering the initial protonation sites of the charge states (an idea that relates to the mobile proton model⁵⁸ and references therein). Additionally, it should be noted that the energy required to produce the same fragment ions from different precursors is different; thus, it might be expected that different populations of conformers of the same fragment would be observed for different charge states.

The observations that multiple conformers exist for fragment ions and appear to vary in abundance depending upon the length

(58) Wysocki, V. H.; Tsapralis, G.; Smith, L. L.; Brei, L. A. *J. Mass Spectrom.* **2000**, *35*, 1399–1406.

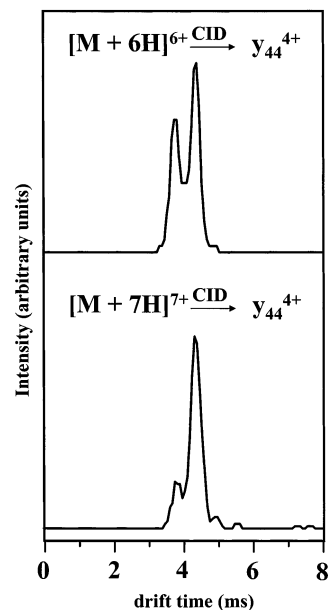


Figure 6. Drift time distributions for the y_{44}^{4+} fragment ion generated from the $[M + 6H]^{6+}$ (top) and $[M + 7H]^{7+}$ (bottom) parent ions of ubiquitin.

and precursor, provide a number of interesting new opportunities for studying protein conformations in the gas phase. Studies associated with understanding structural transitions that occur as amino acids are added or removed from the polymer chain are currently underway in our laboratory.

ACKNOWLEDGMENT

This work is supported by a grant from the National Science Foundation (Grant no. CHE-0078737). E.R.B. is supported by a grant to the Indiana University/Purdue University Indiana Instrumentation Institute (the III) from the Indiana 21st Century Fund. The authors also acknowledge Cherokee S. Hoaglund-Hyzer and J. Mitchell Wells (Purdue University) for their insight about instrumentation and CID of protein ions.

Received for review May 6, 2002. Accepted July 31, 2002.

AC020300U